

## Quasi-three dimensional analysis on the flushing mechanism of sandbar at a river mouth

M. Tateyama

*Graduate School of Science and Engineering, Chuo University, Japan*

T. Uchida & S. Fukuoka

*Research and Development Initiative, Chuo University, Japan*

**ABSTRACT:** The river mouth bars in the Aganogawa River estuary extend toward the center of river from both banks. The sandbar causes the discharge capacity to decrease and the water level to rise. Therefore, it is important to understand flushing mechanism of river mouth sandbar during a flood event. The authors' studies on river floods showed that the flow and bed variation during a flood could be explained by means of a suitable numerical analysis method using temporal changes in observed water surface profiles. The objective of this paper is to clarify the extension process of channel through the river mouth due to the sandbar flushing during a large flood by the quasi-three dimensional numerical analysis, which is capable of estimating the bottom velocity and the non-hydrostatic pressure distributions of flows.

### 1 INTRODUCTION

The sandbars at the mouth of the Aganogawa River extend to the center of the river from both sides of the river bank (Fig. 1). The narrow channel through between the bars was expanded by the largest flood in July, 2011. River mouth sandbar causes the rise of water level and brings large scale bed variation in to surrounding area during the flood. For this reason, it needs to reveal river mouth channel expansion process in the Aganogawa River estuary during the large flood of July, 2011.

The water surface profiles in the estuary area change by the tidal level and deformation of river mouth sandbar. Fukuoka (2011) presented 2D-numerical analysis method using observed water surface profiles to clarify flood phenomena, because the time variation in water surface profiles reflected all kinds of flow resistances during the flood. For example, Okamura et al. (2010) applied analysis methods of a quasi-three-dimensional flood flow and bed variation using observed water surface profiles during a flood in the Ishikarigawa River estuary. Numerical studies on sandbar flashing by flood flows have been conducted for the Aganogawa River (Hosoyamada et al., 2006), the Himekawa River (Sagawa et al., 2007), and the Natorigawa River (Kuwabara et al., 1995), using two dimensional flood flow and bed variation analysis. But the flow near river mouth sandbar is affected by the shape of river mouth and behaves as the three dimensional flow. Secondary



Figure 1. The estuary of the Aganogawa River.

currents generated by streamline curvatures and non-hydrostatic pressure distributions of flood flows become important in determining the sandbar shape. It is difficult to consider these effects by means of a conventional two dimensional calculation method. However, a three dimensional calculation for flood flows and bed variation in rivers are not so easy task because of enormous

computational load. Recently, Uchida & Fukuoka (2012) have developed quasi-three-dimensional computation method (general Bottom Velocity Computation (BVC) method), which is capable of evaluating bottom velocity and non-hydrostatic pressure acting on bed surface. The method would make possible to calculate the flow and bed variation around river mouth sandbar, because the shallow water assumptions such as hydrostatic pressure distribution are not employed in the method.

In this study, the general BVC method together with bed variation analysis in the general curvilinear coordinate system is developed to clarify the effects of river mouth sandbar on flood flow and surrounding bed variation by the flood in July, 2011. Prior to bed variation analysis, fixed bed analysis using the river bed topography observed at 5 months after the 2011 flood is made to know when a channel through between sandbars reaches the maximum during a flood. Then, we discuss the calculation results of bed variation analysis around the sandbars during the flood.

## 2 OBJECTIVE AREA AND FLOOD

### 2.1 Objective area

Figure 1 shows an air photo of the estuary of the Aganogawa River. Figure 2 shows a plan view of objective area from river mouth to 16.0 km where observation stations of water level and discharge are located. The river mouth sandbars are formed around 0.0 km. Because of the bed gradient of 1/1000 to 1/10000, the salt water reaches to the distance 14.0 km from the mouth under the normal flow condition. Figure 3 shows distribution of particle sizes sampled at the estuary (Fig. 1). No. 1 to

No. 6 are located on the sandbars. No. 7 to No. 9 are in the river channel. Most bed materials consist of medium or fine sand. The water level observation systems at the Aganogawa River estuary consist of water level stations of Mastugasaki (1.2 km), Kurumiyama (5.0 km), and ten water level gauges, and provide the temporal water surface profiles that reflect changes in sea level and flood discharge, the sandbars deformation, and estuarine bed variation. The systems worked well in obtaining data of the time variation in the water surface profiles during the largest flood of the Aganogawa River at July, 2011.

### 2.2 Objective flood

The heavy rainfall which caused the flood of 2011 recorded the largest rainfall until now. Many river structures damaged severely such as levee failures and revetment breaks. The maximum discharge

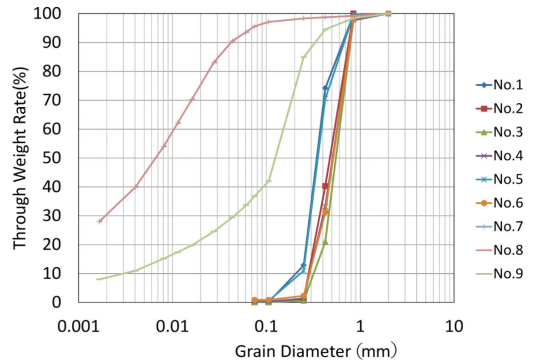


Figure 3. Particle size accumulation curves in the Aganogawa River estuary.

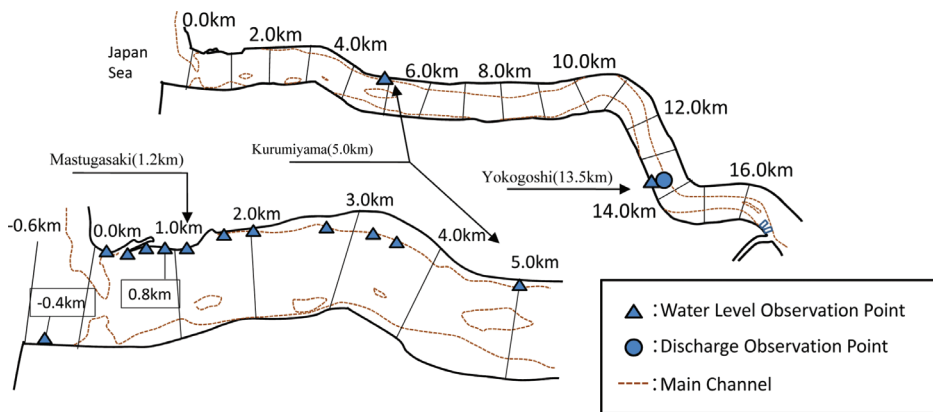


Figure 2. Plan view of objective area and the observation stations of water level and discharge hydrographs.

was observed about 11,000 m<sup>3</sup>/s in the Yokogoshi observation station (13.5 km). It was comparable with the design flood discharge 13,100 m<sup>3</sup>/s. Figure 4 shows observed water level hydrographs of the 2011 flood and the 2004 flood which had been the largest flood until the 2011 flood measured at the Yokogoshi observation station in the Aganogawa River. The 2011 flood water level and discharge were more than those of the 2004 flood, and the maximum water levels were close to H.W.L. We can see three peak discharges in the 2011 flood. This paper calls the three peaks 'Peak 1', 'Peak 2', and 'Peak 3' in chronological order. Figure 4 shows two shore lines surveyed at 5 months before and 5 months after the 2011 flood. The shore lines were defined by the level of 0.5 T.P.m. The markedly eroded shore line is seen despite the measurement of 5 months after the flood.

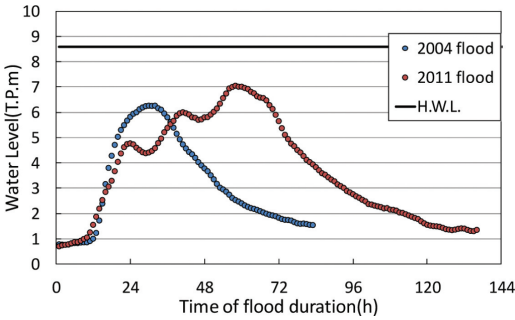


Figure 4. Observed water level on Yokogoshi (13.5 km) water level and discharge observation station.

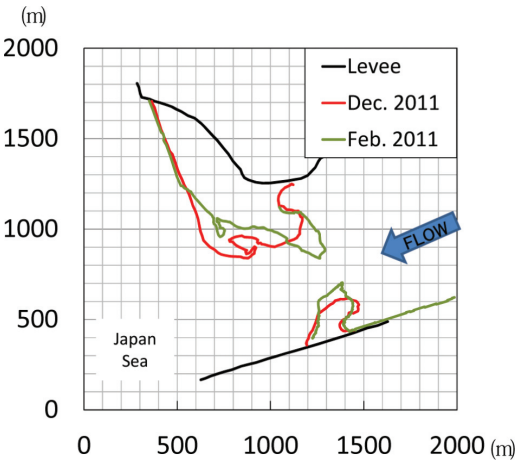


Figure 5. Shore line before and after the 2011 flood defined by the level of 0.5 T.P.m.

### 3 ANALISIS METHOD

#### 3.1 Flood flow analysis method

To calculate three dimensional flow and bed variations around river mouth sandbar, pressure intensity and shear stress acting on bed surface must be appropriately evaluated. We develop the BVC method in the general curvilinear coordinate system. In the BVC method, bottom velocity is solved semi-directly without computing vertical velocity and pressure distributions, using the bottom velocity equation (Eq. 1) derived by depth integrating horizontal vorticity:

$$u_{bi} = u_{si} - \varepsilon_{ij3} \Omega_j h - \frac{\partial W h}{\partial x_i} + w_s \frac{\partial z_s}{\partial x_i} - w_b \frac{\partial z_b}{\partial x_i} \quad (1)$$

where,  $i, j = 1, 2 (x, y)$ ;  $z$  = vertical axis;  $u_{bi}$  = bottom velocity;  $u_{si}$  = water surface velocity;  $\Omega_j$  = depth-average vorticity;  $h$  = water depth;  $W$  = depth-average vertical velocity;  $w_s$  = water surface vertical velocity;  $w_b$  = bottom vertical velocity;  $z_s$  = water surface level;  $z_b$  = bottom level;  $w_s$  and  $w_b$  are defined by the kinematic boundary conditions on water surface and bottom surfaces:

$$w_{(s,b)} = \frac{\partial z_{(s,b)}}{\partial t} + u_i \frac{\partial z_{(s,b)}}{\partial x_i} \quad (2)$$

To evaluate bottom velocity in Equation (1), the general BVC method solves simultaneously depth integrated continuity equation (Eq. 4), depth-averaged velocity (Eq. 5 and 6), depth-averaged vorticity (Eq. 8), water surface velocity (Eq. 9 and 10), depth-average vertical velocity (Eq. 11) and bottom pressure (Eq. 12) by assuming vertical velocity distribution:

$$u'_i = u_i - U_i = \Delta u_i (12\eta^3 - 12\eta^2 + 1) - \delta u_i (4\eta^3 - 3\eta^2) \quad (3)$$

where,  $U_i$  = depth averaged velocity;  $\Delta u_i = u_{si} - U_i$ ;  $\delta u_i = u_{si} - u_{bi}$ ;  $\eta = (z_s - z)/h$ .

To apply the BVC method to flood flow analysis, we employ the general curvilinear coordinates system. The time variation in water depth is calculated by depth integrated continuity Equation (4). The depth-averaged velocity equation (Eq. 5 and 6) has terms of the horizontal shear stress due to vertical velocity distribution and pressure deviation from hydrostatic pressure distribution. In this paper, the  $\xi, \eta$  directional momentum equations described by physical components are used.

$$\frac{\partial h}{\partial t} + \frac{\partial \Delta \eta U_\xi h}{\partial \xi} + \frac{\partial \Delta \xi U_\eta h}{\partial \eta} = 0 \quad (4)$$

( $\xi$ direction)

$$\begin{aligned}
& h \frac{\partial U_\xi}{\partial t} + U_\xi h \frac{\partial U_\xi}{\partial \xi} + U_\eta h \frac{\partial U_\xi}{\partial \eta} \\
& - \tilde{J} \left( U_\eta - U_\xi \cos \theta^{\eta\xi} \right) \left( U_\xi h \frac{\partial \theta^\xi}{\partial \xi} + U_\eta h \frac{\partial \theta^\xi}{\partial \eta} \right) \\
& = -\tau_{b\xi} - gh \left( \frac{\partial z_s}{\partial \xi} + \cos \theta^{\eta\xi} \frac{\partial z_s}{\partial \eta} \right) \\
& - \left( \frac{\partial h d p_0}{\partial \xi} + \cos \theta^{\eta\xi} \frac{\partial h d p_0}{\partial \eta} \right) \\
& - d p_b \left( \frac{\partial z_b}{\partial \xi} + \cos \theta^{\eta\xi} \frac{\partial z_b}{\partial \eta} \right) \\
& + \frac{1}{J} \left\{ \frac{\partial}{\partial \xi} (\Delta \eta \cdot h \tau_{\xi\xi}) + \frac{\partial}{\partial \eta} (\Delta \xi \cdot h \tau_{\xi\eta}) \right\} \\
& - \tilde{J} h \left\{ \left( -\tau_{\xi\xi} \cos \theta^{\eta\xi} + \tau_{\xi\eta} \right) \frac{\partial \theta^\xi}{\partial \xi} \right. \\
& \left. + \left( -\tau_{\xi\eta} \cos \theta^{\eta\xi} + \tau_{\eta\eta} \right) \frac{\partial \theta^\xi}{\partial \eta} \right\}
\end{aligned} \tag{5}$$

( $\eta$ direction)

$$\begin{aligned}
& h \frac{\partial U_\eta}{\partial t} + U_\xi h \frac{\partial U_\eta}{\partial \xi} + U_\eta h \frac{\partial U_\eta}{\partial \eta} \\
& + \tilde{J} \left( U_\xi - U_\eta \cos \theta^{\eta\xi} \right) \left( U_\xi h \frac{\partial \theta^\eta}{\partial \xi} + U_\eta h \frac{\partial \theta^\eta}{\partial \eta} \right) \\
& = -\tau_{b\eta} - gh \left( \frac{\partial z_s}{\partial \eta} + \cos \theta^{\eta\xi} \frac{\partial z_s}{\partial \xi} \right) \\
& - \left( \frac{\partial h d p_0}{\partial \eta} + \cos \theta^{\eta\xi} \frac{\partial h d p_0}{\partial \xi} \right) \\
& - d p_b \left( \frac{\partial z_b}{\partial \eta} + \cos \theta^{\eta\xi} \frac{\partial z_b}{\partial \xi} \right) \\
& + \frac{1}{J} \left\{ \frac{\partial}{\partial \eta} (\Delta \eta \cdot h \tau_{\eta\eta}) + \frac{\partial}{\partial \xi} (\Delta \eta \cdot h \tau_{\xi\eta}) \right\} \\
& - \tilde{J} h \left\{ \left( -\tau_{\eta\eta} \cos \theta^{\eta\xi} + \tau_{\xi\eta} \right) \frac{\partial \theta^\eta}{\partial \eta} \right. \\
& \left. + \left( -\tau_{\xi\eta} \cos \theta^{\eta\xi} + \tau_{\xi\xi} \right) \frac{\partial \theta^\eta}{\partial \xi} \right\}
\end{aligned} \tag{6}$$

where,  $U_\xi, U_\eta$  = depth-average velocity in  $\xi, \eta$  directions;  $J, \tilde{J}$  = coordinate transform Jacobian matrix;  $g$  = gravity acceleration;  $\Delta \xi, \Delta \eta$  = length of grid interval in  $\xi, \eta$  directions;  $\tau_{b\xi}, \tau_{b\eta}$  = bed shear stress;  $d p$  = pressure deviation from hydrostatic pressure distribution ( $p = \rho g(z_s - z) + d p$ );  $d p_0$  = depth averaged  $d p$ ;  $d p_b = d p$  on bottom;  $\tau_{\xi\xi}, \tau_{\eta\eta}, \tau_{\xi\eta}$  = horizontal shear stress. All velocity vectors and shear stress tensors indicate physical components. This paper follows the definition of the general curvilinear coordinate system indicated by Fukuoka (2005). The horizontal

shear stress composes of turbulence and vertical velocity distribution. The Cartesian form:

$$\tau_{ij} = 2\nu_t \left( \frac{\partial U_i}{\partial x_j} - \frac{\partial U_j}{\partial x_i} \right) - \overline{u_i' u_j'} \tag{7}$$

where,  $\nu_t$  = eddy viscosity calculated by zero equation model with the assumption of locally-balanced turbulence kinetic energy due to vertical velocity distribution;  $\overline{u_i' u_j'}$  = depth averaged  $u_i' u_j'$ .

The depth integrated horizontal vorticity equations are:

$$\begin{aligned}
\frac{\partial J \Omega_i h}{\partial t} & = J \left( ER_{\sigma i} + P_{\omega i} + \frac{\partial h \Delta \eta D_{\omega \xi i}}{\partial \xi} + \frac{\partial h \Delta \xi D_{\omega \eta i}}{\partial \eta} \right) \\
ER_{\sigma i} & = u_{si} \omega_{s\sigma} - u_{bi} \omega_{b\sigma} \\
P_{\omega i} & = C_{p\omega} v_{tb} (\omega_{bei} - \omega_{bi}) / h, \quad C_{p\omega} = \kappa' \alpha, \quad \alpha = \kappa / 6 \\
D_{\omega \xi i} & = -U_\xi \Omega_i + U_i \Omega_\xi + \overline{\omega' u_i'} - \overline{\omega' u_i' \xi} \\
& + \frac{\nu_t}{\sigma_\omega} \left( \frac{\partial \Omega_i}{\partial \xi} + \cos \theta^{\eta\xi} \frac{\partial \Omega_i}{\partial \eta} \right) \\
D_{\omega \eta i} & = -U_\eta \Omega_i + U_i \Omega_\eta + \overline{\omega' u_i'} - \overline{\omega' u_i' \eta} \\
& + \frac{\nu_t}{\sigma_\omega} \left( \frac{\partial \Omega_i}{\partial \eta} + \cos \theta^{\eta\xi} \frac{\partial \Omega_i}{\partial \xi} \right)
\end{aligned} \tag{8}$$

where,  $D_{\omega \xi i}, D_{\omega \eta i}$  = depth-average vorticity flux due to advection, rotation, deformation and diffusion;  $ER_{\sigma i}$  = rotation of vertical vorticity;  $\omega_{s\sigma}, \omega_{b\sigma}$  = rotation of  $u_{si}, u_{bi}$ ;  $\nu_{tb}$  = eddy viscosity on bottom converted to depth averaged scale;  $\omega_{bei}$  = equilibrium vorticity on bottom calculated by the bed shear stress;  $\kappa$  = Karman constant number;  $\sigma_\omega = 1.0$ ;  $\overline{\omega \xi' u_i'}, \overline{\omega_i' u \xi'}$  = depth averaged  $\omega \xi' u_i', \omega_i' u \xi'$ ;  $\omega \xi', \omega_i'$  = deviation from depth-average vorticity. The vertical vorticity distribution is defined as the differential form of Equation (3).

The water surface velocity equations are:

$$\begin{aligned}
& \left( \xi \text{direction} \right) \\
& \frac{\partial u_{s\xi}}{\partial t} + u_{s\xi} \frac{\partial u_{s\xi}}{\partial \xi} + u_{s\eta} \frac{\partial u_{s\xi}}{\partial \eta} \\
& - \tilde{J} \left( u_{s\eta} - u_{s\xi} \cos \theta^{\eta\xi} \right) \left( u_{s\xi} \frac{\partial \theta^\xi}{\partial \xi} + u_{s\eta} \frac{\partial \theta^\xi}{\partial \eta} \right) \\
& = - \left\{ g - \left( \frac{\partial d p}{\partial z} \right)_{z=z_s} \right\} \left( \frac{\partial z_s}{\partial \xi} + \cos \theta^{\eta\xi} \frac{\partial z_s}{\partial \eta} \right) + P_{s\xi}
\end{aligned} \tag{9}$$

$$\begin{aligned}
& (\eta \text{ direction}) \\
& \frac{\partial u_{s\eta}}{\partial t} + u_{s\xi} \frac{\partial u_{s\eta}}{\partial \xi} + u_{s\eta} \frac{\partial u_{s\eta}}{\partial \eta} \\
& + \tilde{J} \left( u_{s\xi} - u_{s\eta} \cos \theta^{\eta\xi} \right) \left( u_{s\xi} \frac{\partial \theta^{\eta\xi}}{\partial \xi} + u_{s\eta} \frac{\partial \theta^{\eta\xi}}{\partial \eta} \right) \\
& = - \left\{ g - \left( \frac{\partial dp}{\partial z} \right)_{z=z_s} \right\} \left\{ \left( \frac{\partial z_s}{\partial \tilde{\eta}} + \cos \theta^{\eta\xi} \frac{\partial z_s}{\partial \xi} \right) \right\} + P_{s\eta}
\end{aligned} \tag{10}$$

where,  $u_{s\xi}$ ,  $u_{s\eta}$  = water surface velocity in contravariant  $\xi$ ,  $\eta$  directions;  $P_{s\xi}$ ,  $P_{s\eta}$  = shear stress acting on very thin layer under the water surface.

An equation of depth-average vertical velocity is obtained by continuity equation (Eq. 4) and bottom velocity equation (Eq. 1) (Uchida & Fukuoka, 2012). For the general curvilinear coordinates system:

$$\begin{aligned}
& \frac{\partial \Delta \eta \cdot h^2 \phi_\xi}{J \partial \xi} + \frac{\partial \Delta \xi \cdot h^2 \phi_\eta}{J \partial \eta} + \frac{\phi^p - \phi}{k_1} = 0 \\
& (\phi_\xi, \phi_\eta) = \left( \frac{\partial \phi}{\partial \xi} + \cos \theta^{\eta\xi} \frac{\partial \phi}{\partial \tilde{\eta}}, \frac{\partial \phi}{\partial \eta} + \cos \theta^{\eta\xi} \frac{\partial \phi}{\partial \xi} \right)
\end{aligned} \tag{11}$$

where,  $\phi = (Wh)^{n+1} - (Wh)^n$ ;  $\phi^p = (Wh)^p - (Wh)^n$ ;  $k_1 = 1/20$ ;  $(Wh)^p$  = predicted depth integrated vertical velocity by using  $\delta u_i^p$ ;  $\delta u_i^p$  = predicted velocity difference between water surface and bottom velocity by Equation (1) with  $(Wh)^n$ ,  $n$  = time step.

The bottom pressure intensity is evaluated by integrating the vertical momentum equation. The equation is described in the general curvilinear coordinate system by omitting the terms of unsteady and horizontal shear stress:

$$\frac{dp_b}{\rho} = U_\xi h \frac{\partial W}{\partial \xi} + U_\eta h \frac{\partial W}{\partial \eta} + \tau_{b\xi} \frac{\partial z_b}{\partial \xi} + \tau_{b\eta} \frac{\partial z_b}{\partial \eta} \tag{12}$$

The vertical distribution of pressure deviation  $dp$  is defined by a linear distribution for evaluating the non-hydrostatic pressure term in the depth-average velocity equation (Eq. 5 and 6) and the pressure distribution at water surface in water surface velocity equation (Eq. 9 and 10).

### 3.2 Bed variation analysis method

In this study, bed variation analysis considers both suspended load and bed load. Because particle sizes are almost uniform, this study assumes bed material as uniform  $d_{50}$  (0.5 mm) sand. The temporal variations in bed elevation are evaluated from sediment continuity equation (Eq. 13).

$$\begin{aligned}
& \frac{\partial z_b}{\partial t} + \frac{1}{(1-\lambda)J} \left( \frac{\partial \Delta \eta \cdot q_{B\xi}}{\partial \xi} + \frac{\partial \Delta \xi \cdot q_{B\eta}}{\partial \eta} \right) \\
& + \frac{1}{(1-\lambda)} (c_b w_0 - q_{su}) = 0
\end{aligned} \tag{13}$$

where,  $\lambda$  = void ratio;  $q_{B\xi}$ ,  $q_{B\eta} = \xi, \eta$  directional contravariant vector of bed load rate;  $c_b$  = sediment concentration on the reference boundary calculated by the Lane-Kalinske formula (1972);  $w_0$  = settling velocity calculated by the Rubey formula (1933),  $q_{su}$  = suspended sediment rate calculated by the Itakura-Kishi formula (1980). The bed load rate is calculated by the Ashida-Michiue formula (1972). Suspended sediment load is calculated by 2D advection and diffusion equation (Eq. 14).

$$\begin{aligned}
& \frac{\partial C}{\partial t} + \frac{1}{J} \left( \frac{\partial \Delta \eta \cdot U^\xi C}{\partial \xi} + \frac{\partial \Delta \xi \cdot U^\eta C}{\partial \eta} \right) \\
& = \frac{\partial}{\partial \xi} \left( \varepsilon_s \cdot \frac{\partial C}{\partial \xi} \right) + \frac{\partial}{\partial \tilde{\eta}} \left( \varepsilon_s \cdot \frac{\partial C}{\partial \tilde{\eta}} \right) \\
& + \cos \theta^{\eta\xi} \left\{ \frac{\partial}{\partial \xi} \left( \varepsilon_s \cdot \frac{\partial C}{\partial \tilde{\eta}} \right) + \frac{\partial}{\partial \tilde{\eta}} \left( \varepsilon_s \cdot \frac{\partial C}{\partial \xi} \right) \right\} \\
& + \frac{\varepsilon_s}{\tilde{J}} \left\{ \frac{\partial C}{\partial \xi} \frac{\partial \theta^{\eta\xi}}{\partial \tilde{\eta}} + \frac{\partial C}{\partial \tilde{\eta}} \frac{\partial \theta^{\eta\xi}}{\partial \xi} \right\} + q_{su(z=z_b)} - c_b w_0
\end{aligned} \tag{14}$$

where,  $\varepsilon_s$  = diffusion coefficient ( $\varepsilon_s = \nu_t$ ).

### 3.3 Calculation conditions

Table 1 shows the calculation conditions. Figure 6 shows about 5 m computational mesh around the river mouth. Figure 7 shows upstream and downstream boundary conditions which were observed water level hydrographs at Yokogoshi (13.5 km) and Niigata West Port, respectively. The bed resistance is evaluated by the equivalent roughness  $k_s$ (m). The  $k_s$  values are determined to reproduce water surface profiles for Peak 2 and Peak 3. Initial cross-sectional profiles are important for the deformation analysis of river mouth sandbar. So, initial cross-sectional profiles set for this analysis are made carefully by the data surveyed at 200 m intervals, contour map of ocean floor topography observed in March 2008 (for the area downstream from -0.6 km), a detailed bathymetry map below 0.5 T.P.m between -0.6 km and 1.0 km surveyed in February, 2011, and images of CCTV camera installed near river mouth and aerial photos taken during July, 2011 flood. Figure 10(a) shows the initial bed topography used for the bed variation analysis.

Table 1. Calculation conditions.

Range of calculation		Fixed bed analysis	Bed variation analysis
		Sea of Japan~6.0 km	Sea of Japan~16.0 km
Boundary condition	Upstream end	Kurumiyama water level observation point (5.0 km)	Yokogoshi water level observation point (13.5 km)
	Downstream end	Niigata West Port tidal level	
Mesh size	Sea:	30 m × 30 m Observed conter map of Japan Sea in Mar. 2008	5 m × 5 m [-0.6 km~1.0 km]
	River:	Observed cross section bed at 200 m intervals in Dec. 2011	(Under 0.5 T.P.m) Observed conter map around the bars (Upper 0.5 T.P.m) Observed cross section bed at 200 m intervals in Jul. 2009
Initial bed topography data	Flood plane	Reed: 2.97, Wooded: 0.6 + Permeability coefficient, the playing ground & cultivation: 0.2, others: 0.6	[1.2 km~16.0 km] Observed cross section bed at 200 m intervals in Jul. 2009
	Equivalent roughness $k_s$ (m)	Low water channel 0.005	[Japan Sea~5.0 km] 0.005 →(Change on 5 hours before Peak 3) 0.005, 0.04 (Only -0.6 km~1.0 km) [5.0 km~9.0 km] 0.005 →(Change on 5 hours before Peak 3) 0.02~0.074 [9.0 km~] 0.074
Bed material		Uniform particle diameter: 0.5 mm	

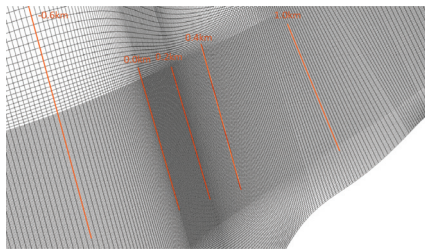


Figure 6. The mesh shape around the river mouth that is adapted for bed variation analysis.

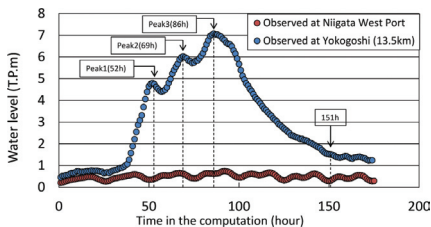


Figure 7. Boundary conditions in the movable bed computation.

## 4 CALCULATION RESULTS AND DISCUSSION

### 4.1 Fixed bed analysis

The river mouth sandbars changed in shape and reduced in size with time by the flood. At first, the fixed bed analysis was carried out using bed topography measured after the 2011 flood. This analysis was made to estimate roughly when the maximum deformation of sandbars occurred. Since the flow resistance due to sandbar deformation becomes smaller, water levels around the bar are calculated lower by means of the fixed bed analysis. Figure 8 shows observed and computed water surface profiles. At the Peak 1, especially for 0.0 km~2.0 km section, the computed water levels are about 0.5 m lower than observed one. This result reveals that the presence of river mouth sandbar makes the great deal of water level rise. At the Peak 2, the difference between observed and computed water levels is smaller than that of peak 1. But the computed water levels are still low compared to the observed ones. Hence, it is considered that the river mouth bar has not yet fully deformed. At the Peak 3, on the other hand, the

computed water level is higher than the observed water level. The fixed bed analysis suggests that the river mouth cross-sectional area should be expanded around the time of Peak 3 because the cross-sectional area around river mouth after the flood would become smaller than that of Peak 3 by the river flow and the action of sea wave.

#### 4.2 Movable bed variation analysis

Figure 9 shows observed and computed water surface profiles at Peak 1 (52 h), Peak 2 (69 h), and Peak 3 (86 h). The time indicated is described on the water level hydrograph in Figure 7. Equivalent roughness coefficient  $k_s$  is determined to coincide

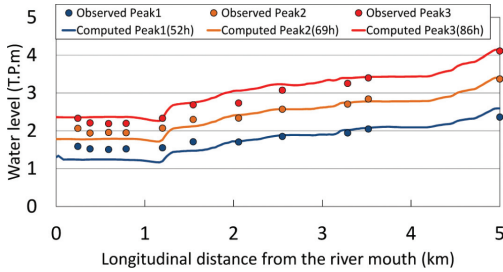


Figure 8. Comparisons between observed and computed water surface profiles (fixed bed condition).

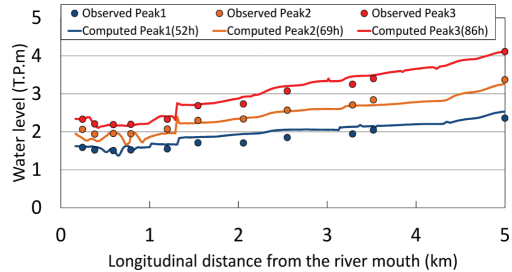


Figure 9. Comparisons between observed and computed water surface profiles (movable bed condition).

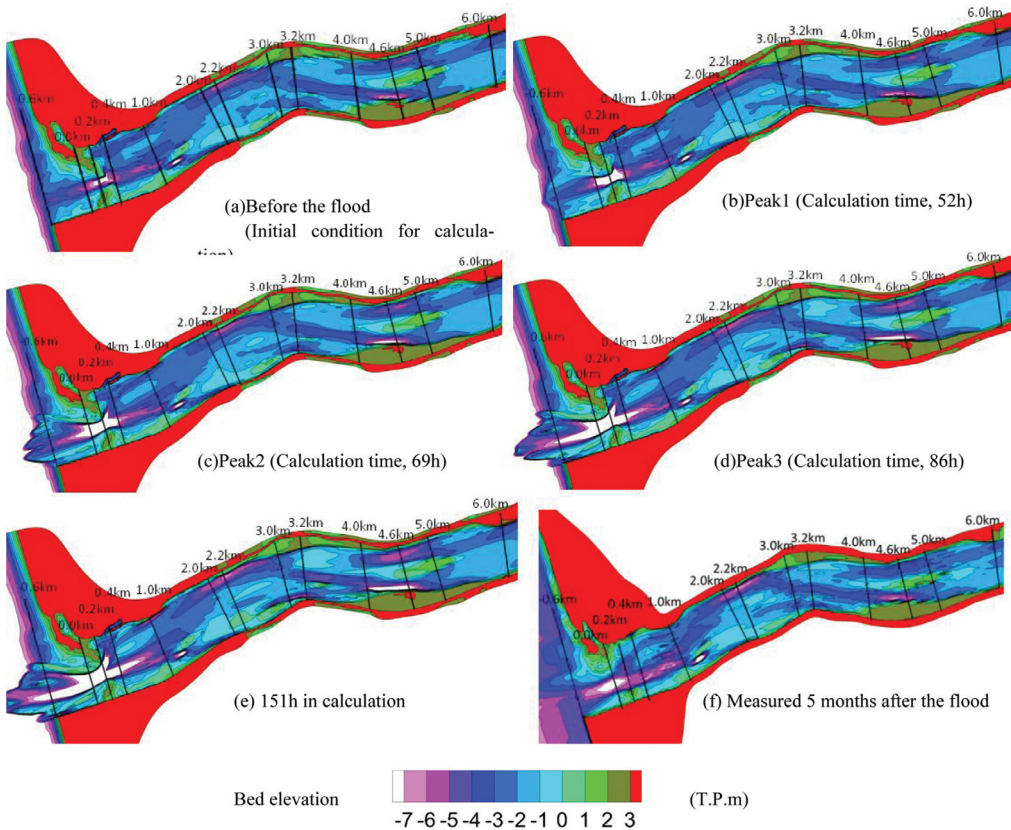


Figure 10. Comparison of observed and computed morphologies at the peak discharge times, before and after the flood.

with water surface profiles at each time. Value of  $k_s$  is assumed 0.005 (m) at the downstream and upstream reaches of 1.2 km till the time of Peak 2. After the Peak 3, the respective values  $k_s$  are 0.04 (m) and 0.005 (m). The step change in water surface around 1.2 km indicates the rise of water levels due to the reduction of the cross-section.

Figure 10 shows calculated bed topographies for (a) the initial condition before the flood, (b) Peak 1 (52 h), (c) Peak 2 (69 h), (d) Peak 3 (86 h), and (e) 151 h, and (f) measured 5 months after the flood. Figure 11 shows observed and computed temporal variations in the cross sectional forms at the river

mouth sandbar (0.2 km, 0.25 km) and in the main channel (2.2 km, 3.2 km, 4.6 km). Figure 11 also shows water levels at the river mouth corresponding to each flood time by dotted lines.

The computed cross-sectional area at 0.2 km is widening over 100 m and deepening over 10 m until the time of Peak 3 as shown in Figure 10. This is because the flood at Peak 3 flowed over the right river mouth sandbar with the steep slope for rather long time. The 151 h computational cross-sectional profile shows further channel widening due to the erosion of the right sandbar. The computation time of 151 h would be regarded as the

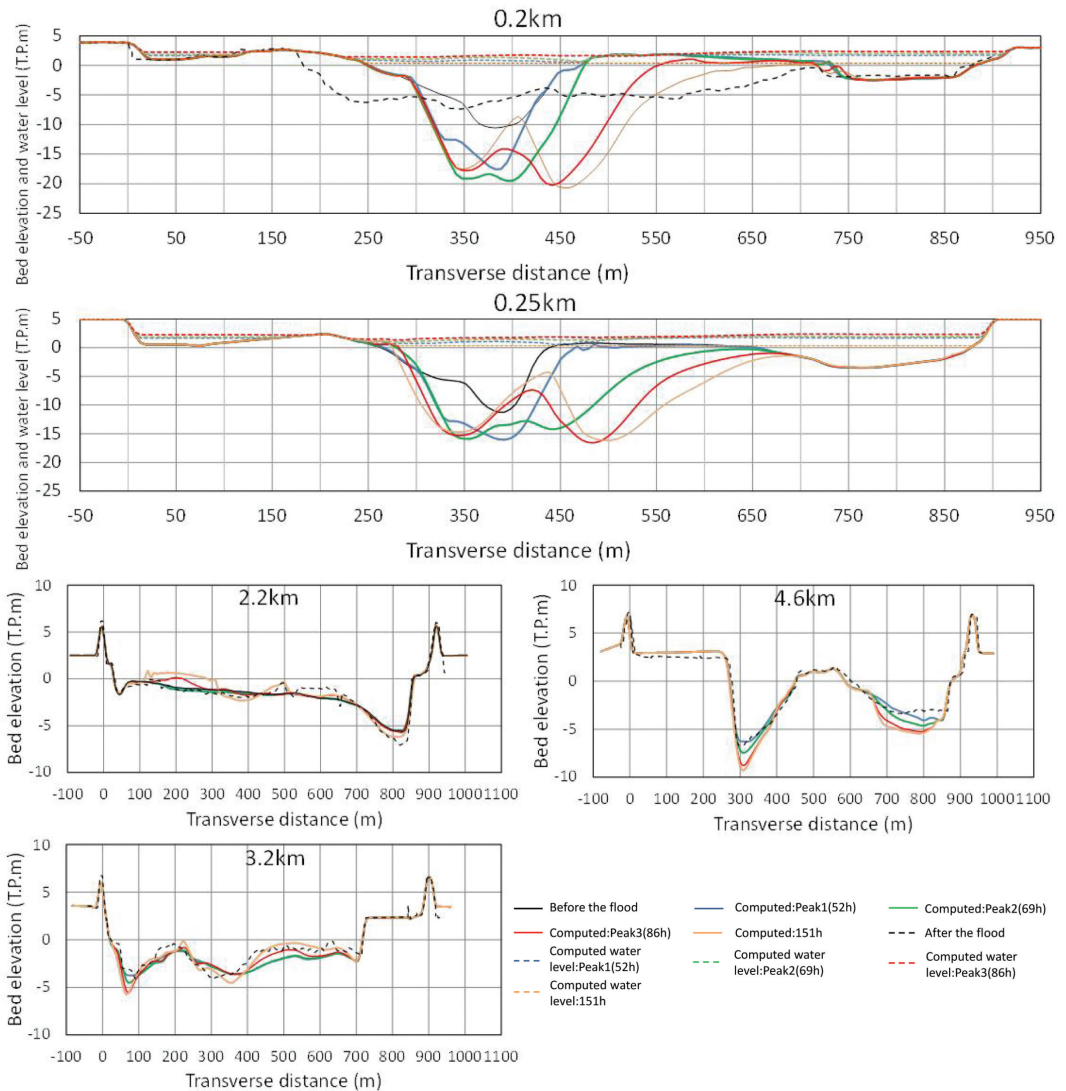


Figure 11. Temporal variation of computed and observed cross-sections before and after the flood.

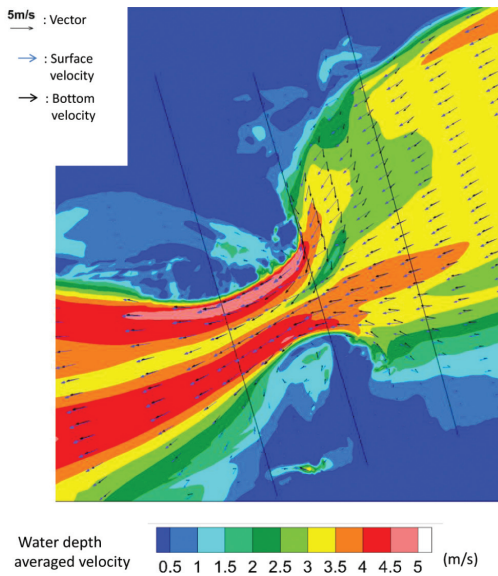


Figure 12. Computed water surface, bottom and water depth averaged velocity at Peak 3 around the river mouth (movable bed condition).

end of the falling stage of the flood. Figures 10(d) and (e) show that a bar moved into the river mouth from the upstream around the time of Peak 3 and caused a large amount of sediment deposition in the channel center of the river mouth. On the other hand, the left sandbar at 0.2 km in 151 h computation time does not alter in shape and differ from measured one. Main reason is because the overflow beyond the left sandbar did not occur during the flood as seen in Figure 11. The cross-section profile of 0.2 km is the survey data of the seaside of the left sandbar. The cross-sectional profile of the left sandbar at 0.25 km is that the riverside (0.25 km) is found to be expanded from the initial channel form. However, the water level seems to be not beyond the bed during the flood. However, survey data of the left sandbar before the flood was not accurate enough compared to initial data of the right sandbar. CCTV camera was not set near the left sandbars and flood images taken. This reveals that initial river mouth sandbar topography and camera images during floods play important roles for the accuracy of the analysis results of sandbar deformation.

River bed variations in the upstream of 1.2 km are described as follows. Depositions (right side at 3.0 km–3.2 km, and center at 2.2 km) and erosions (right side at 2.0 km–2.2 km) are compared by bed topographies computed in 151h and observed after the flood. Computed bed variations agree well with observed ones on the whole. However,

151 h computed bed level around 4.6 km is deeper than the observed bed level after the flood. The resistances due to vegetated bank and bridge piers around 4.6 km are not considered in the present calculation.

Here, Figure 12 shows the velocity field around the river mouth at Peak 3. There are clear directional gaps between water surface velocity and bottom velocity, so it means that velocity distributions were very complex by the considerable streamline curvatures near river mouth sandbars. The general BVC method reproduces the process of observed sandbar deformation. The BVC method together with bed variation analysis is usable for estimating the bed and bank variations in the three dimensional flow. However computed scouring depth at the last stage is larger than observed one. It could be related that the bed topography was measured 5 months after the flood. Hence, immediate observations of the estuarine sandbar topography after the flood are expected in the future study.

## 5 CONCLUSIONS

In this paper, two kinds of numerical computations using quasi-three dimensional analysis method (BVC method) were conducted to clarify the deformation mechanism of the river mouth sandbars by the flood of 2011 in the Aganogawa River. One is the analysis using fixed bed topography measured after the flood. The other is the flood flow and bed variation analysis by new computation method. The main conclusions are given as follows:

1. Fixed bed analysis using bed topography after the flood is a useful method for estimating when a channel through between sandbars reached the maximum cross-sectional area during a flood.
2. The BVC method using temporal changes in water surfaces profiles and bed variation analysis provides a good explanation for deformation of the river mouth sandbars and the flushing mechanism of sandbar by a large flood.
3. Detailed survey of river mouth sandbars before the flood and immediate survey after the flood are very important to estimate accurately river mouth bar deformation during a flood.

## REFERENCES

- Fukuoka, S. 2005. *Flood hydraulics and channel design*, Tokyo: Morikita Publishing Company.
- Fukuoka, S. 2011. What is the Fundamentals of design-utilization of visible techniques of sediment laden-flood flows. *Advances in River Engineering* 17: 83–88.

- Hosoyamada, T., Sano, T., Noda, T., Sakai, Y., & Sakawa, H. 2006. A numerical study for flashing of sandbars by flood in the Aganogawa river mouth. *Advances in River Engineering* 12: 73–78.
- Kuwabara, N., Tanaka, H., Satoh, K., & Shutoh, N. 1995. *Proceedings of Coastal Engineering*, JSCE, Vol. 42: 596–600.
- Okamura, S., Okabe, K. & Fukuoka, S. 2011. Bed variation analysis using the sediment transport formula considering the effect of river width and cross sectional form—in the case of 1981 flood of the Ishikari river—. *Advances in River Engineering* 17: 119–124.
- Sagawa, T., Ohya, Y., Ichikawa, S., Takeuchi, Y., & Yamashita, T. 2007. Study on numerical simulation and factor analysis of flushing river mouth. *Annual Journal of Hydraulic Engineering* 51: 955–960.
- Uchida, T., & Fukuoka, S. 2012. Bottom velocity computation method by depth integrated model without shallow water assumption. *Annual Journal of Hydraulic Engineering* 56: I\_1225–I\_1230.